Hamiltonian Conservation Laws and Finite-Difference Simulations for a Nonlinearly Coupled Generalized Schrödinger–KdV System

Hongyi Wu *

Department of Mathematics, University of California, Berkeley, Berkeley, CA, USA

* Corresponding Author Email: hongyi_wu@berkeley.edu

Abstract. This paper studies a Hamiltonian generalized Schrödinger–KdV system generated by a nonlinear long-wave coupling potential. Starting from an energy functional with a smooth coupling function $\phi(V)$, we derive a matched coupled system involving the terms $\phi(V)U$ and $(\phi'(V)|U|^2)_x$, with the quadratic case $\phi(V) = V + \kappa V^2$ used for numerical simulations. Under periodic boundary conditions, we prove conservation of the Schrödinger mass, the long-wave mean, a generalized momentum, and the Hamiltonian energy. A fully discrete finite-difference method based on central differences and the implicit midpoint rule is then constructed. The scheme exactly preserves the discrete mass and discrete long-wave mean, while the generalized momentum and energy are monitored as diagnostic quantities. Numerical experiments confirm the expected second-order convergence behavior and illustrate the long-time boundedness of the monitored invariant errors.

Keywords: Schrödinger–KdV system; long-short wave interaction; Hamiltonian structure; conservation law; finite difference method; implicit midpoint rule.

1. Introduction

Coupled dispersive systems provide reduced mathematical models for nonlinear interactions between wave modes of different scales. A particularly important example is the Schrödinger–KdV system, in which a complex nonlinear Schrödinger component describes a short-wave envelope and a real Korteweg–de Vries component describes a long-wave mode. Such systems appear in the study of plasma waves, capillary-gravity waves, and nonlinear wave modulation. Classical derivations and related long-short wave models can be traced back to early work on coupled electron-plasma and ion-acoustic waves and on the interaction of short and long water waves [1, 2, 3, 4].

A standard Schrödinger–KdV model may be written as

$$\begin{cases} iU_t + U_{xx} = \beta|U|^2U + \gamma_1\phi(V)U, \\ V_t + V_{xxx} + \nu VV_x = \gamma_2\,\partial_x(\phi'(V)|U|^2). \end{cases} \tag{1}$$

Here U is a complex-valued short-wave envelope and V is a real-valued long-wave field. The term VU represents the modulation of the short wave by the long wave, while the derivative source term $(|U|^2)_x$ describes the feedback of the short wave on the long-wave equation. A central feature of this model is that the two coupling terms are not independent: they are compatible with an underlying Hamiltonian structure and with several conservation laws.

The analysis of Schrödinger–KdV systems has been developed in many directions. Local and global well-posedness, low-regularity theory, and periodic problems have been studied in [5, 6, 7, 8]. Existence and stability of solitary waves, as well as generalized or multicomponent Schrödinger–gKdV systems, have also been investigated [9, 10, 11]. These works show that conservation laws such as mass, momentum, and energy are not only formal identities but also important tools in analytical theory.

The present work is motivated by nonlinear long-short wave interactions in which the influence of the long wave on the short-wave frequency is not necessarily linear. When the long-wave amplitude is not sufficiently small, higher-order corrections to the modulation relation may arise. A natural way to model such a correction is to replace the linear coupling potential V by a nonlinear function $\phi(V)$. In order to avoid destroying the conservation structure, however, the modification must be introduced

at the Hamiltonian level rather than inserted separately into the equations. This leads to the generalized system

$$\begin{cases} iU_t + U_{xx} = \beta|U|^2U + \gamma_1\phi(V)U, \\ V_t + V_{xxx} + \nu VV_x = \gamma_2\,\partial_x(\phi'(V)|U|^2). \end{cases} \tag{2}$$

The second equation contains the variational flux generated by the same coupling potential as the first equation. Thus, the nonlinear term in the Schrödinger component and the feedback term in the KdV component form a matched pair.

Although the formulation is written for a general smooth coupling function, this paper focuses on the quadratic case $\phi(V) = V + \kappa V^2$, which can be viewed as a second-order approximation of a nonlinear long-wave modulation law. The parameter κ measures the strength of the quadratic correction. For $\kappa = 0$, the model reduces to the classical linearly coupled Schrödinger–KdV system. For $\kappa \neq 0$, the Schrödinger equation contains the additional modulation term κV^2U, and the KdV equation contains the corresponding flux correction $\partial_x(2\kappa V|U|^2)$.

From a numerical perspective, long-time simulations of dispersive Hamiltonian systems are sensitive to the treatment of invariants. Conservative finite-difference, finite-element, compact finite-difference, and local discontinuous Galerkin methods have been proposed for Schrödinger–KdV type systems and related dispersive equations [12, 13, 14, 15, 16]. More generally, geometric numerical integration, discrete-gradient methods, and average-vector-field methods provide systematic frameworks for preserving Hamiltonian or dissipative structures [17, 18, 19, 20, 21]. In the present paper, we deliberately adopt a simple finite-difference method based on central differences and the implicit midpoint rule. This choice keeps the method transparent and allows us to separate what can be proved exactly at the discrete level from what is only observed numerically.

The main contributions of this paper are as follows.

1. A Hamiltonian extension of the Schrödinger–KdV system is formulated through a nonlinear long-wave coupling potential $\phi(V)$, with the quadratic potential $\phi(V) = V + \kappa V^2$ taken as the principal model in this work.

2. For the continuous model, conservation of the Schrödinger mass, long-wave mean, generalized momentum, and Hamiltonian energy is proved under periodic boundary conditions.

3. A fully discrete central-difference/implicit-midpoint scheme is constructed. Discrete summation-by-parts identities are used to prove exact preservation of the discrete mass and discrete long-wave mean.

4. The local consistency of the scheme is recorded at the formal level. Long-time conservation-error tests and convergence tests are used to assess the numerical behavior of the method.

The paper is organized as follows. Section 2 formulates the Hamiltonian model and proves the continuous conservation laws. Section 3 presents the fully discrete method, the discrete summation-by-parts formulas, discrete conservation of mass and mean value, the Picard iteration, and a formal consistency statement. Section 4 reports the numerical experiments, including the discrete error quantities used in the plots. Section 5 concludes the paper. Appendix A contains detailed term-by-term proof of energy conservation.

2. Hamiltonian Model and Continuous Conservation Laws

2.1. Hamiltonian formulation

Let the periodic spatial domain be $\Omega = (-L, L)$ with $L > 0$. Let $U: \Omega \times [0,T] \to \mathbb{C}$ and $V: \Omega \times [0,T] \to \mathbb{R}$, where U is the short-wave envelope and V is the long-wave component. For a real smooth coupling potential $\phi \in C^2(\mathbb{R})$, define the Hamiltonian energy.

$$E_\phi(U,V) := \int_\Omega \left[|U_x|^2 + \frac{\beta}{2}|U|^4 + \gamma_1\phi(V)|U|^2 + \frac{\gamma_1}{2\gamma_2}|V_x|^2 - \frac{\gamma_1\nu}{6\gamma_2}V^3\right] dx. \tag{3}$$

Using the Wirtinger variational derivative with respect to $\overline{U}$ and V, we obtain

$$\frac{\delta E_\phi}{\delta \overline{U}} = -U_{xx} + \beta|U|^2U + \gamma_1\phi(V)U \tag{4}$$

$$\frac{\delta E_\phi}{\delta V} = \gamma_1\phi'(V)|U|^2 - \frac{\gamma_1}{\gamma_2}V_{xx} - \frac{\gamma_1\nu}{2\gamma_2}V^2 \tag{5}$$

Therefore, the Hamiltonian-type system

$$iU_t = \frac{\delta E_\phi}{\delta \overline{U}}, \qquad V_t = \frac{\gamma_2}{\gamma_1}\partial_x\frac{\delta E_\phi}{\delta V} \tag{6}$$

can be written as

$$\begin{cases} iU_t + U_{xx} = \beta|U|^2U + \gamma_1\phi(V)U, \\ V_t + V_{xxx} + \nu VV_x = \gamma_2\,\partial_x(\phi'(V)|U|^2) \end{cases} \tag{7}$$

In this paper, we focus on $\phi(V) = V + \kappa V^2$, $\phi'(V) = 1 + 2\kappa V$, where $\kappa \in \mathbb{R}$ measures the strength of the quadratic long-wave coupling. It follows from (7) that

$$\begin{cases} iU_t + U_{xx} = \beta|U|^2U + \gamma_1(V + \kappa V^2)U, \\ V_t + V_{xxx} + \nu VV_x = \gamma_2\,\partial_x[(1 + 2\kappa V)|U|^2] \\ U(x,0) = U_0(x), \\ V(x,0) = V_0(x). \end{cases} \tag{8}$$

When $\kappa = 0$ and $\nu = 1$, this reduces to the classical Schrödinger–KdV coupling. The quadratic term is therefore a Hamiltonian extension of the classical model rather than an unrelated perturbation.

2.2. Continuous conservation laws

All calculations below are performed on the periodic domain $\Omega = (-L, L)$. For smooth periodic functions, boundary terms vanish after integration by parts. In particular,

$$\int_\Omega \partial_x F\,dx = 0, \qquad \int_\Omega f_x\,g\,dx = -\int_\Omega f\,g_x\,dx \tag{9}$$

Theorem 2.1. *Let $\phi \in C^2(\mathbb{R})$ and let (U, V) be a sufficiently smooth periodic solution of (7). Then the following quantities are independent of time:*

$$M(U) := \int_\Omega |U|^2\,dx, \qquad Q(V) := \int_\Omega V\,dx \tag{10}$$

$$P(U,V) := \mathrm{Im}\int_\Omega \overline{U}\,U_x\,dx - \frac{\gamma_1}{2\gamma_2}\int_\Omega V^2\,dx, \tag{11}$$

$$E_\phi(U,V) := \int_\Omega \left[|U_x|^2 + \frac{\beta}{2}|U|^4 + \gamma_1\phi(V)|U|^2 + \frac{\gamma_1}{2\gamma_2}|V_x|^2 - \frac{\gamma_1\nu}{6\gamma_2}V^3\right]dx. \tag{12}$$

Proof. We give the main verification. The detailed term-by-term energy calculation is recorded in Appendix A. First, from the Schrödinger equation, $U_t = iU_{xx} - i\beta|U|^2U - i\gamma_1\phi(V)U$. Thus

$$\frac{d}{dt}M(U) = 2\mathrm{Re}\int_\Omega U_t\,\overline{U}\,dx = 2\mathrm{Re}\left[i\int_\Omega U_{xx}\,\overline{U}\,dx - i\beta\int_\Omega |U|^4\,dx - i\gamma_1\int_\Omega \phi\,(V)|U|^2dx\right]. \tag{13}$$

The three integrals in brackets are real after integration by parts; hence the real part is zero and $\frac{d}{dt}M(U) = 0$. Second, using the conservative form of the long-wave equation $V_t = -V_{xxx} - \nu VV_x + \gamma_2\,\partial_x(\phi'(V)|U|^2)$, we obtain

$$\frac{d}{dt}Q(V) = -\int_{\Omega} V_{xxx}\, dx - \nu \int_{\Omega} V\, V_x\, dx + \gamma_2 \int_{\Omega} \partial_x \left(\phi'(V)|U|^2\right) dx = 0. \tag{14}$$

Third, set

$$S(U) := \mathrm{Im} \int_{\Omega} \overline{U}\, U_x\, dx, \qquad g(U,V) := \beta|U|^2 + \gamma_1 \phi(V) \tag{15}$$

Since $iU_t + U_{xx} = gU$, a standard integration-by-parts calculation gives

$$\frac{d}{dt}S(U) = -\gamma_1 \int_{\Omega} \phi'(V)|U|^2 V_x\, dx \tag{16}$$

On the other hand,

$$\frac{1}{2}\frac{d}{dt}\int_{\Omega} V^2\, dx = -\gamma_2 \int_{\Omega} \phi'(V)|U|^2 V_x\, dx \tag{17}$$

Equations (16) and (17) imply $\frac{d}{dt}P(U,V) = 0$.

Finally, by (4)– (5),

$$\frac{d}{dt}E_{\phi}(U,V) = 2\mathrm{Re} \int_{\Omega} \frac{\delta E_{\phi}}{\delta \overline{U}} U_t\, dx + \int_{\Omega} \frac{\delta E_{\phi}}{\delta V} V_t\, dx. \tag{18}$$

Using the Hamiltonian form (6), this becomes

$$\frac{d}{dt}E_{\phi}(U,V) = 2\mathrm{Re} \int_{\Omega} i\, U_t \overline{U_t}\, dx + \frac{\gamma_2}{\gamma_1}\int_{\Omega} \frac{\delta E_{\phi}}{\delta V}\partial_x\left(\frac{\delta E_{\phi}}{\delta V}\right) dx \tag{19}$$

$$\frac{d}{dt}E_{\phi}(U,V) = 2\mathrm{Re} \int_{\Omega} i\,|U_t|^2 dx + \frac{\gamma_2}{2\gamma_1}\int_{\Omega} \partial_x\left[\left(\frac{\delta E_{\phi}}{\delta V}\right)^2\right] dx = 0. \tag{20}$$

The first term is zero because $i|U_t|^2$ is purely imaginary, and the second term vanishes by periodicity. Hence the energy is conserved.

Corollary 2.2. *Taking $\phi(V) = V + \kappa V^2$ in Theorem 2.1 gives the four conservation laws for the quadratically coupled system (8). In this case the Hamiltonian is denoted by $E_{\kappa}(U,V)$.*

3. Fully Discrete Finite-Difference Method

This section gives the fully discrete finite-difference formulation used in the computations. We first introduce the periodic grid and the summation-by-parts identities, then state the implicit-midpoint scheme, prove the two discrete invariants preserved exactly by the scheme, and finally describe the Picard iteration used to solve the nonlinear algebraic system.

3.1. Grid, Operators, and Discrete Summation by Parts

Let $x_j = -L + jh,\ j = 0,1,\dots,N-1,\ h = \frac{2L}{N}$, and $t_n = n\tau,\ n = 0,1,\dots,N_t$. For periodic grid functions $Z_{j+N} = Z_j$, define

$$D_x Z_j = \frac{Z_{j+1} - Z_{j-1}}{2h}, \qquad D_{xx} Z_j = \frac{Z_{j+1} - 2Z_j + Z_{j-1}}{h^2}, \tag{21}$$

And

$$D_{xxx} Z_j = D_x D_{xx} Z_j = \frac{Z_{j+2} - 2Z_{j+1} + 2Z_{j-1} - Z_{j-2}}{2h^3} \tag{22}$$

We also define

$$\delta_t Z_j^n = \frac{Z_j^{n+1} - Z_j^n}{\tau}, \qquad Z_j^{n+\frac{1}{2}} = \frac{Z_j^{n+1} + Z_j^n}{2} \tag{23}$$

For complex grid functions we use both the bilinear pairing and the Hermitian discrete inner product

$$(X,Y)_h = h\sum_{j=0}^{N-1} X_j\, Y_j, \qquad \langle X,Y\rangle_h = h\sum_{j=0}^{N-1} X_j\, \overline{Y_j} \tag{24}$$

The Hermitian inner product is used in the discrete mass argument, while the bilinear pairing is convenient for real-valued summation identities.

Lemma 3.1 (Discrete summation by parts). *For periodic grid functions, the central difference* operator *satisfies the bilinear identity* $(D_x Z, Y)_h = -(Z, D_x Y)_h$, *and, for complex grid functions, the Hermitian* identity $\langle D_x Z, Y\rangle_h = -\langle Z, D_x Y\rangle_h$. *Moreover,*

$$h\sum_{j=0}^{N-1} D_x\, Z_j = 0, \qquad h\sum_{j=0}^{N-1} D_{xxx}\, Z_j = 0 \tag{25}$$

The operator D_{xx} *is self-adjoint with respect to* $\langle\cdot,\cdot\rangle_h$, *and* $\langle D_{xx}Z, Z\rangle_h \in \mathbb{R}$. *In particular, the contribution of* D_{xx} *to the imaginary part in the discrete Schrödinger mass calculation is zero.*

Proof. The identities follow by shifting summation indices and using the periodic condition $Z_{j+N} = Z_j$. For example,

$$(D_x Z, Y)_h = \frac{1}{2}\sum_j \left(Z_{j+1} - Z_{j-1}\right) Y_j = -\frac{1}{2}\sum_j Z_j \left(Y_{j+1} - Y_{j-1}\right) = -(Z, D_x Y)_h \tag{26}$$

The Hermitian identity is obtained in the same way after taking the complex conjugate in the second argument. The formulas for the sums of $D_x Z$ and $D_{xxx} Z$ are telescoping sums on the periodic grid. The self-adjointness of D_{xx} follows from the same index-shift argument.

3.2. Implicit Midpoint Scheme

The fully discrete scheme used in this paper is

$$\begin{cases} i\delta_t U_j^n + D_{xx} U_j^{n+\frac{1}{2}} = \beta \left|U_j^{n+\frac{1}{2}}\right|^2 U_j^{n+\frac{1}{2}} + \gamma_1 \left[V_j^{n+\frac{1}{2}} + \kappa \left(V_j^{n+\frac{1}{2}}\right)^2\right] U_j^{n+\frac{1}{2}}, \\ \delta_t V_j^n + D_{xxx} V_j^{n+\frac{1}{2}} + \frac{\nu}{2} D_x \left[\left(V_j^{n+\frac{1}{2}}\right)^2\right] = \gamma_2 D_x \left[\left(1 + 2\kappa V_j^{n+\frac{1}{2}}\right)\left|U_j^{n+\frac{1}{2}}\right|^2\right] \end{cases} \tag{27}$$

The KdV nonlinearity is written in conservative form, $VV_x = \frac{1}{2}\partial_x(V^2)$, which is essential for the discrete mean-value calculation. This conservative placement of all spatial derivative terms is the key discrete feature used in the following mass and mean-value conservation proofs.

3.3. Discrete Conservation of Mass and Mean Value

Proposition **3.2 (Discrete long-wave mean).** *Under the periodic boundary conditions, scheme (27) satisfies* $Q_h^{n+1} = Q_h^n$ *with* $Q_h^n := h\sum_{j=0}^{N-1} V_j^n$.

Proof. Multiply the second equation of (27) by h and sum over j. By Lemma 3.1, the sums of $D_{xxx}V^{n+1/2}$, $D_x\left(\left(V^{n+1/2}\right)^2\right)$, and $D_x\left(\left(1 + 2\kappa V^{n+1/2}\right)\left|U^{n+1/2}\right|^2\right)$ are all zero. Hence

$$h\sum_j \frac{V_j^{n+1}-V_j^n}{\tau}=0 \tag{28}$$

Which implies $Q_h^{n+1}=Q_h^n$.

Proposition 3.3 (Discrete Schrödinger **mass).** *Under the periodic boundary conditions, scheme (27) satisfies* $M_h^{n+1}=M_h^n$ *with* $M_h^n=h\sum_{j=0}^{N-1}\left|U_j^n\right|^2$.

Proof. Let $G_j^{n+1/2}=\beta\left|U_j^{n+1/2}\right|^2+\gamma_1\left(V_j^{n+1/2}+\kappa\left(V_j^{n+1/2}\right)^2\right)$, which is real-valued. The first equation of (27) can be written as $i\delta_t U_j^n=-D_{xx}U_j^{n+1/2}+G_j^{n+1/2}U_j^{n+1/2}$. Taking the discrete inner product with $U^{n+1/2}$ and then taking imaginary parts gives

$$\mathrm{Im}\langle i\delta_t U^n,U^{n+1/2}\rangle_h=\mathrm{Im}\langle -D_{xx}U^{n+1/2},U^{n+1/2}\rangle_h+\mathrm{Im}\left(h\sum_j G_j^{n+1/2}\left|U_j^{n+1/2}\right|^2\right) \tag{29}$$

The right-hand side is zero because both terms are real. On the left-hand side,

$$\mathrm{Im}\left(i\delta_t U_j^n\overline{U_j^{n+1/2}}\right)=\mathrm{Re}\left(\delta_t U_j^n\overline{U_j^{n+1/2}}\right)=\frac{\left|U_j^{n+1}\right|^2-\left|U_j^n\right|^2}{2\tau} \tag{30}$$

Therefore $\frac{M_h^{n+1}-M_h^n}{2\tau}=0$, and the discrete mass is conserved.

3.4. Picard Iteration for the Nonlinear System

At each time step, scheme (27) leads to a nonlinear algebraic system because the midpoint values appear inside $|U|^2$, $\phi(V)$, and $\phi'(V)|U|^2$. In the MATLAB experiments, this nonlinear system is solved by a Picard fixed-point iteration. Given U^n and V^n, the initial iterate is chosen as $U^{n+1,0}=U^n$, $V^{n+1,0}=V^n$. For $\ell=0,1,2,\ldots$, define

$$U^{n+1/2,\ell}=\frac{U^{n+1,\ell}+U^n}{2},\qquad V^{n+1/2,\ell}=\frac{V^{n+1,\ell}+V^n}{2} \tag{31}$$

The nonlinear coefficients are frozen at the previous midpoint iterate. In the quadratic case, this means that the coefficients

$$\phi\left(V_j^{n+1/2,\ell}\right)=V_j^{n+1/2,\ell}+\kappa\left(V_j^{n+1/2,\ell}\right)^2,\qquad \phi'\left(V_j^{n+1/2,\ell}\right)=1+2\kappa V_j^{n+1/2,\ell} \tag{32}$$

And the nonlinear amplitude factors are evaluated from the previous iterate. The next iterate is then obtained by solving the resulting linearized midpoint equations for $U^{n+1,\ell+1}$ and $V^{n+1,\ell+1}$. The iteration stops when

$$\frac{\|\,U^{n+1,\ell+1}-U^{n+1,\ell}\,\|_{2,h}+\|\,V^{n+1,\ell+1}-V^{n+1,\ell}\,\|_{2,h}}{1+\|\,U^{n+1,\ell+1}\,\|_{2,h}+\|\,V^{n+1,\ell+1}\,\|_{2,h}}<\mathrm{Tol} \tag{33}$$

Unless otherwise stated, $\mathrm{Tol}=10^{-12}$ is used.

Algorithm 1. Picard iteration for one implicit-midpoint step.

Given U^n,V^n, set $U^{n+1,0}=U^n$ and $V^{n+1,0}=V^n$.

For $\ell=0,1,2,\ldots$, form the midpoint iterates $U^{n+1/2,\ell}$ and $V^{n+1/2,\ell}$.

Freeze all nonlinear coefficients at the current midpoint iterate.

Solve the resulting linearized discrete system for $U^{n+1,\ell+1}$ and $V^{n+1,\ell+1}$.

Stop if the relative difference in (33) is below Tol; otherwise continue.

The nonlinear iteration error may affect both convergence tests and conservation-error plots. In the long-time and spatial experiments, the stopping tolerance is fixed at 10^{-12}. In the refined

temporal convergence experiment reported below, the tolerance is tightened to 10^{-13} and the MATLAB computation records the iteration history. The linearized systems in each Picard update are solved by an LU decomposition of the time-step-dependent sparse matrices, with MATLAB backslash used as a fallback. The iteration statistics for the refined temporal convergence test are reported in Table 1. All time steps in this test reached the prescribed tolerance. For stronger coupling parameters or larger time steps, a damp Newton method can be used if the Picard iteration stagnates.

3.5. Formal consistency discussion

Assume that the exact solution (U, V) is sufficiently smooth and periodic, for instance with enough time derivatives and at least six spatial derivatives on Ω. Substituting the exact solution into the fully discrete equations produces local residuals $T_{U,j}^n$ and $T_{V,j}^n$. The implicit midpoint rule is second-order accurate in time for smooth solutions. The central difference D_{xx} approximates ∂_{xx} with second-order accuracy, and the composition $D_{xxx} = D_x D_{xx}$ approximates ∂_{xxx} with second-order accuracy. Since the nonlinear terms are smooth functions of U, $\overline{U}$, and V, Taylor expansion gives the formal estimate

$$\max_{j,n}\left|T_{U,j}^n\right| + \max_{j,n}\left|T_{V,j}^n\right| \le C(\tau^2 + h^2) \tag{34}$$

for a constant C depending on the smooth exact solution but not on h or τ. This discussion explains the expected second-order behavior tested in the numerical section. A full convergence theorem would additionally require stability estimates for the nonlinear fully discrete system.

4. Numerical Experiments

4.1. Numerical setting and error measures

This section reports MATLAB experiments for quadratic coupling potential $\phi(V) = V + \kappa V^2$. The purpose of the numerical part is twofold. First, it checks whether the quantities proved at the continuous and discrete levels behave as predicted in computation. Second, it examines whether the finite-difference scheme displays the expected convergence behavior. Unless otherwise stated, the parameters are $\beta = \gamma_1 = \gamma_2 = \nu = 1$, $\kappa = 0.5$, $\Omega = (-20,20)$. The initial data are $U_0(x) = 0.8\,\mathrm{sech}(x)e^{0.8ix}$, $V_0(x) = 0.5\,\mathrm{sech}^2(x)$.

These data are exponentially localized rather than strictly periodic. On the computational interval $(-20,20)$, their boundary values and derivatives are very small; they are therefore treated as periodic data in the finite-difference computation. This localization-periodization approximation is reported explicitly because the theoretical analysis assumes periodic boundary conditions.

Table 1. Numerical configurations used in reported experiments.

Experiment	Main settings
Long-time conservation	$N = 256$, $\tau = 0.005$, $T = 200$, $\kappa = 0.5$; relative errors of M_h, Q_h, $P_{\kappa,h}$, and $E_{\kappa,h}$ are monitored.
Temporal convergence	$\Omega = (-\pi, \pi)$, $N = 2048$, $T = 0.1$, strictly periodic initial data $U_0(x) = 0.5(1 + 0.1\cos x)e^{ix}$ and $V_0(x) = 0.2\cos x$; $\tau = 0.0125/2^m$ for $m = 0,1,\ldots,7$; the reference step is $\tau_{\mathrm{ref}} = \tau_{\min}/4$ and the Picard tolerance is 10^{-13}.
Spatial convergence	$T = 0.05$, $\tau = 5 \times 10^{-5}$, $N = 64,96,128,192,256,384,512,768$; the reference grid is $N_{\mathrm{ref}} = 1536$.

The following discrete quantities are used in numerical tests:

$$M_h^n = h\sum_{j=0}^{N-1}\left|U_j^n\right|^2, \qquad Q_h^n = h\sum_{j=0}^{N-1} V_j^n \tag{35}$$

$$P_{\kappa,h}^{n} = h\mathrm{Im}\sum_{j=0}^{N-1}\overline{U_j^n}\,D_x U_j^n - \frac{\gamma_1}{2\gamma_2}h\sum_{j=0}^{N-1}\left(V_j^n\right)^2 \tag{36}$$

$$E_{\kappa,h}^{n} = h\sum_{j=0}^{N-1}\left[\left|D_x U_j^n\right|^2 + \frac{\beta}{2}\left|U_j^n\right|^4 + \gamma_1\left(V_j^n + \kappa\left(V_j^n\right)^2\right)\left|U_j^n\right|^2 + \frac{\gamma_1}{2\gamma_2}\left|D_x V_j^n\right|^2 - \frac{\gamma_1\nu}{6\gamma_2}\left(V_j^n\right)^3\right] \tag{37}$$

For $I \in \{M, Q, P, E\}$, the relative error is defined by $e_I(t_n) = \frac{|I_h^n - I_h^0|}{1+|I_h^0|}$. We will use these definitions to evaluate long-time invariant errors and convergence behavior.

4.2. Long-time conservation errors

Figure 1 reports the relative errors of the four discrete quantities for $N = 256$, $\tau = 0.005$, $T = 200$, and $\kappa = 0.5$. The discrete mass and long-wave mean remain small, with errors near 10^{-10}–10^{-9} and 10^{-13}–10^{-12}, respectively. This behavior is consistent with Propositions 3.2 and 3.3. The generalized momentum and energy errors are larger, approximately of order 10^{-3}, but remain bounded over the interval shown. The present method is therefore best described as a finite-difference scheme that exactly preserves the discrete mass and long-wave mean, while using the discrete generalized momentum and energy as diagnostics. It is not an exact energy-preserving method for $E_{\kappa,h}^{n}$.

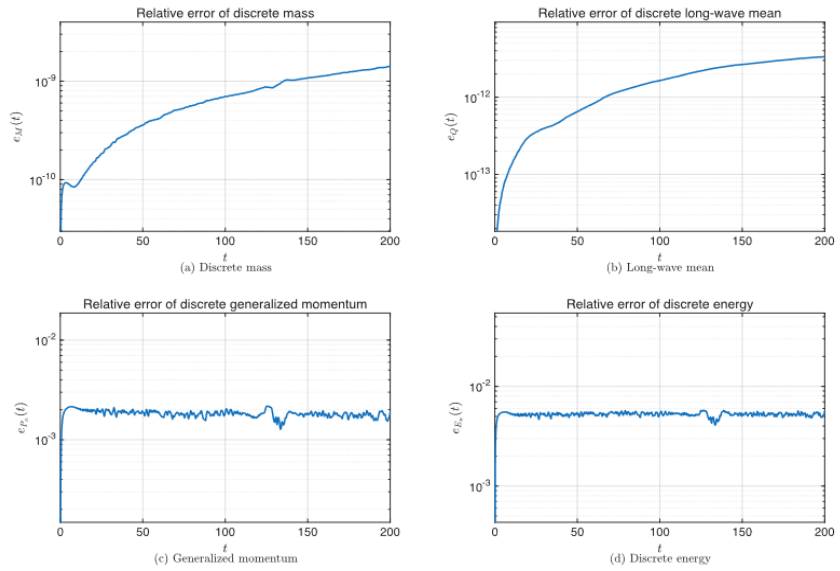


Figure 1. Relative errors of the discrete mass, long-wave mean, generalized momentum, and energy for $N = 256$, $\tau = 0.005$, $T = 200$, and $\kappa = 0.5$.

Implementation method. The spatial derivatives are discretized by central differences and the solution is advanced by the implicit midpoint rule. At each time step, the nonlinear equations are solved by Picard iteration. The four discrete quantities are evaluated at every time level, and the relative errors $e_M(t)$, $e_Q(t)$, $e_P(t)$, and $e_E(t)$ are displayed in logarithmic scale.

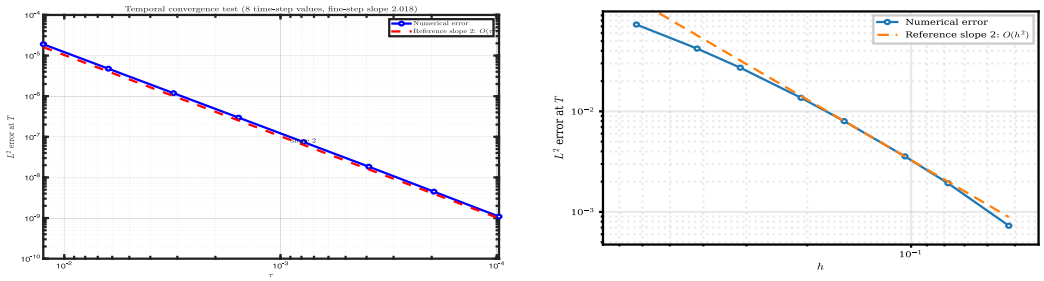
4.3. Temporal and spatial convergence

The temporal convergence test was recomputed with a strictly periodic initial condition in order to match the periodic boundary condition assumed in the analysis. The computational interval is $\Omega = (-\pi, \pi)$, the spatial grid is fixed at $N = 2048$, and the final time is shortened to $T = 0.1$ so that the temporal discretization error is not polluted by long-time effects. The initial data are $U_0(x) = 0.5(1 + 0.1\cos x)e^{ix}$, $V_0(x) = 0.2\cos x$. Eight time-step values $\tau = 0.0125/2^m$, $m = 0,1,\ldots,7$, are tested. The reference solution is computed with $\tau_{\mathrm{ref}} = \tau_{\min}/4$, and the Picard tolerance is tightened to 10^{-13}. The MATLAB run reports that all Picard iterations converged to the prescribed tolerance.

Figure 2(a) shows the terminal-time discrete L^2 error and the reference line $O(\tau^2)$. The fitted slope based on all eight time-step values is approximately 2.011, and the fitted slope based on the refined six time-step values is approximately 2.018. This confirms the expected second-order temporal behavior of the implicit midpoint discretization in the refined periodic setting. The corresponding error values and Picard iteration statistics are listed in Table 2. The maximum number of Picard iterations decreases from 20 to 13 as the time step is refined, and no failed time steps occur.

Table 2. Temporal convergence errors and Picard iteration statistics for the refined periodic test. Here eτ is the terminal-time discrete L² error and Tol = 10^{-13}.

τ	eτ	order	max iter	avg iter	failed steps
0.0125	1.90×10^{-5}	–	20	17.25	0
0.00625	4.75×10^{-6}	1.9993	16	16.00	0
0.00313	1.19×10^{-6}	2.0000	16	16.00	0
0.00156	2.97×10^{-7}	2.0007	15	15.00	0
$7.81E^{-4}$	7.41×10^{-8}	2.0028	15	15.00	0
$3.91E^{-4}$	1.84×10^{-8}	2.0098	14	14.00	0
$1.95E^{-4}$	4.47×10^{-9}	2.0414	14	14.00	0
$9.77E^{-5}$	1.09×10^{-9}	2.0384	13	13.00	0



(a) Temporal convergence (b) Spatial convergence

Figure 2. Convergence test with eight time-step values.

Implementation method. The temporal error is computed as

$$e_{\tau} = \| U_h^{\tau}(T) - U_h^{\mathrm{ref}}(T) \|_{2,h} + \| V_h^{\tau}(T) - V_h^{\mathrm{ref}}(T) \|_{2,h}, \tag{38}$$

The errors are plotted against τ in log-log coordinates and compared with an $O(\tau^2)$ reference line. Compared with the previous localized-data test, the present setting uses strictly periodic data, a finer spatial grid, a smaller final time, a finer reference step, and a stricter nonlinear tolerance.

For the spatial convergence test, a small-time step is fixed, and a fine-grid solution is used as the reference solution. Figure 2(b) shows the terminal-time discrete L^2 error and the reference line $O(h^2)$. The fitted slope is approximately 1.850, which is reasonably close to the second-order behavior expected from the central difference discretization.

The corresponding raw spatial errors and adjacent observed orders are reported in Table 3.

Table 3. Spatial convergence errors and observed orders. Here eh is the terminal-time discrete L² error computed against the fine-grid reference solution with Nref = 1536.

N	h	eh	Order
64	0.625000	7.30×10^{-2}	–
96	0.416667	4.21×10^{-2}	1.358
128	0.312500	2.72×10^{-2}	1.521
192	0.208333	1.36×10^{-2}	1.700
256	0.156250	8.00×10^{-3}	1.854
384	0.104167	3.57×10^{-3}	1.990
512	0.078125	1.93×10^{-3}	2.140
768	0.052083	7.29×10^{-4}	2.399

Implementation method. A reference solution is first computed on a fine spatial grid and then restricted to each coarser grid. The spatial error is defined by

$$e_h = \| U_h(T) - U_{\mathrm{ref}}(T) \|_{2,h} + \| V_h(T) - V_{\mathrm{ref}}(T) \|_{2,h}. \tag{39}$$

For two consecutive mesh sizes, the observed order is computed by order = log (eh, k-1/eh,k) / log(hk-1/hk). The error is plotted against h in log-log coordinates together with the reference line $O(h^2)$. Since the mesh sequence is not purely dyadic and the reference solution is restricted from a finite grid, the adjacent orders show mild variation, while the overall fitted slope remains close to two.

5. Conclusion

This paper studied a Hamiltonian-type generalized Schrödinger–KdV system generated by a nonlinear long-wave coupling potential. The construction yields the matched coupling terms $\phi(V)U$ and $\partial_x(\phi'(V)|U|^2)$, with the quadratic case $\phi(V) = V + \kappa V^2$ serving as the main example. We proved the conservation of the Schrödinger mass, long-wave mean, generalized momentum, and Hamiltonian energy under periodic boundary conditions. A central-difference and implicit-midpoint scheme was then proposed, and the discrete mass and long-wave mean were shown to be exactly preserved. The numerical results confirmed the expected convergence behavior and showed bounded errors for the generalized momentum and energy.

Future work may proceed in two directions. First, more numerical tests should be carried out, including strictly periodic long-time experiments, step-size-dependence tests, and comparisons for different values of κ. Second, it would be natural to construct an energy-preserving fully discrete method, for example by using a discrete-gradient or average-vector-field formulation.

Appendix A. Detailed Energy Conservation Calculation

This appendix gives the direct term-by-term verification of the energy conservation law for the quadratic case. It supplements the shorter Hamiltonian proof in Section 2.2.

For $\phi(V) = V + \kappa V^2$, write $E_\kappa(U,V) = I_1(t) + I_2(t) + I_3(t) + I_4(t) + I_5(t)$, where

$$I_1(t) = \int_\Omega |U_x|^2\,dx, \qquad I_2(t) = \frac{\beta}{2}\int_\Omega |U|^4\,dx, \qquad I_3(t) = \gamma_1 \int_\Omega \phi\,(V)|U|^2 dx,$$
$$I_4(t) = \frac{\gamma_1}{2\gamma_2}\int_\Omega V_x^2\,dx, \qquad I_5(t) = -\frac{\gamma_1 \nu}{6\gamma_2}\int_\Omega V^3\,dx. \tag{40}$$

For the short-wave gradient term,

$$\frac{d}{dt} I_1(t) = \int_\Omega \left(U_{xt}\overline{U_x} + U_x\overline{U_{xt}}\right) dx = 2\mathrm{Re}\int_\Omega U_{xt}\,\overline{U_x}\,dx = 2\mathrm{Re}\int_\Omega (-U_{xx})\,\overline{U_t}\,dx \tag{41}$$

Where the boundary term vanishes because of periodicity. For the quartic short-wave term, since $|U|^2 = U\overline{U}$, we have $\partial_t|U|^2 = U_t\overline{U} + U\overline{U_t} = 2\mathrm{Re}\left(U\overline{U_t}\right)$, and

$$\frac{d}{dt} I_2(t) = \frac{\beta}{2}\int_\Omega \partial_t\,(|U|^4) dx = 2\mathrm{Re}\int_\Omega \beta\,|U|^2 U\overline{U_t}\,dx \tag{42}$$

For the coupling term, the product and chain rules give

$$\frac{d}{dt} I_4(t) = \frac{\gamma_1}{\gamma_2}\int_\Omega V_x\,V_{xt}\,dx = -\frac{\gamma_1}{\gamma_2}\int_\Omega V_{xx}\,V_t\,dx \tag{43}$$

For the long-wave gradient term,

$$\frac{d}{dt} I_4(t) = \frac{\gamma_1}{\gamma_2}\int_\Omega V_x\,V_{xt}\,dx = -\frac{\gamma_1}{\gamma_2}\int_\Omega V_{xx}\,V_t\,dx. \tag{44}$$

For the cubic long-wave term,

$$\frac{d}{dt} I_5(t) = -\frac{\gamma_1 \nu}{2\gamma_2} \int_\Omega V^2 V_t \, dx. \tag{45}$$

Adding the five derivatives yields

$$\begin{aligned} \frac{d}{dt} E_\kappa(U,V) = 2\mathrm{Re} \int_\Omega [-U_{xx} + \beta |U|^2 U + \gamma_1 \phi(V) U] \, \overline{U_t} \, dx \\ + \int_\Omega \left[\gamma_1 \phi'(V) |U|^2 - \frac{\gamma_1}{\gamma_2} V_{xx} - \frac{\gamma_1 \nu}{2\gamma_2} V^2 \right] V_t \, dx. \end{aligned} \tag{46}$$

The two bracketed expressions are exactly $\frac{\delta E_\kappa}{\delta \overline{U}}$ and $\frac{\delta E_\kappa}{\delta V}$. Using $\frac{\delta E_\kappa}{\delta \overline{U}} = iU_t$ and $V_t = \frac{\gamma_2}{\gamma_1} \partial_x \frac{\delta E_\kappa}{\delta V}$, we obtain

$$\frac{d}{dt} E_\kappa(U,V) = 2\mathrm{Re} \int_\Omega i \, |U_t|^2 dx + \frac{\gamma_2}{\gamma_1} \int_\Omega \frac{\delta E_\kappa}{\delta V} \partial_x \left(\frac{\delta E_\kappa}{\delta V} \right) dx \tag{47}$$

$$\frac{d}{dt} E_\kappa(U,V) = 2\mathrm{Re} \int_\Omega i \, |U_t|^2 dx + \frac{\gamma_2}{2\gamma_1} \int_\Omega \partial_x \left[\left(\frac{\delta E_\kappa}{\delta V} \right)^2 \right] dx = 0 \tag{48}$$

The first term is zero because it is the real part of a purely imaginary quantity, and the second term vanishes under periodic boundary conditions.

References

[1] K. Nishikawa, H. Hojo, K. Mima, and H. Ikezi, Coupled nonlinear electron-plasma and ion-acoustic waves, *Physical Review Letters*, 33 (1974), 148–151.

[2] T. Kawahara, N. Sugimoto, and T. Kakutani, Nonlinear interaction between short and long capillary-gravity waves, *Journal of* the *Physical Society of Japan*, 39 (1975), 1379–1386.

[3] D. J. Benney, A general theory for interactions between short and long waves, *Studies in Applied Mathematics*, 56 (1977), 81–94.

[4] K. Appert and J. Vaclavik, Dynamics of coupled solitons, *Physics of Fluids*, 20 (1977), 1845–1849.

[5] A. Arbieto, A. J. Corcho, and C. Matheus, Rough solutions for the periodic Schrödinger–Korteweg–de Vries system, Journal *of Differential Equations*, 230 (2006), 295–336.

[6] A. J. Corcho and F. Linares, Well-posedness for the Schrödinger–Korteweg–de Vries system, *Transactions of the American* Mathematical *Society*, 359 (2007), 4089–4106.

[7] C. Matheus, Global well-posedness of NLS-KdV systems for periodic functions, *Electronic Journal of Differential* Equations, 2007, no. 7, 1–20.

[8] Z. Guo and Y. Wang, On the well-posedness of the Schrödinger–Korteweg–de Vries system, *Journal of Differential Equations*, 249 (2010), 2500–2520.

[9] F. S. de Oliveira, Well-posedness and existence of bound states for a coupled Schrödinger-gKdV system, Nonlinear *Analysis: Theory, Methods & Applications*, 73 (2010), 2686–2698.

[10] J. P. Albert and S. Bhattarai, Existence and stability of a two-parameter family of solitary waves for an NLS-KdV system, arXiv preprint arXiv:1212.3902, 2012.

[11] S. Bhattarai, A. J. Corcho, and M. Panthee, Well-posedness for multicomponent Schrödinger-gKdV systems and stability of solitary waves with prescribed mass, arXiv preprint arXiv:1509.08188, 2015.

[12] D. Bai and L. Zhang, The finite element method for the coupled Schrödinger-KdV equations, *Physics Letters A*, 373 (2009), 2237–2244.

[13] A. Golbabai and A. Safdari-Vaighani, A meshless method for numerical solution of the coupled Schrödinger-KdV equations, *Computing*, 92 (2011), 225–242.

[14] P. Amorim and M. Figueira, Convergence of a numerical scheme for a coupled Schrödinger–KdV system, Revista *Matemática Complutense*, 26 (2013), 409–426.

[15] S. Xu and J. Yan, A conservative local discontinuous Galerkin method for the Schrödinger-KdV system, *Communications in* Computational *Physics*, 14 (2013), 1287–1310.

[16] J. Qiu, D. Han, and H. Zhou, A general conservative eighth-order compact finite difference scheme for the coupled Schrödinger-KdV equations, *AIMS Mathematics*, 8 (2023), 10596–10618.

[17] O. Gonzalez, Time integration and discrete Hamiltonian systems, *Journal of Nonlinear Science*, 6 (1996), 449–467.

[18] R. I. McLachlan, G. R. W. Quispel, and N. Robidoux, Geometric integration using discrete gradients, *Philosophical Transactions of the Royal Society A*, 357 (1999), 1021–1045.

[19] G. R. W. Quispel and D. I. McLaren, A new class of energy-preserving numerical integration methods, *Journal of Physics A:* Mathematical *and Theoretical*, 41 (2008), 045206.

[20] E. Hairer, C. Lubich, and G. Wanner, *Geometric Numerical Integration: Structure-Preserving Algorithms for Ordinary* Differential *Equations*, 2nd ed., Springer, Berlin, 2006.

[21] E. Celledoni, V. Grimm, R. I. McLachlan, D. I. McLaren, D. O'Neale, B. Owren, and G. R. W. Quispel, preserving energy resp. dissipation in numerical PDEs using the average vector field method, *Journal of Computational Physics*, 231 (2012), 6770–6789.